FRP INTERNATIONAL

The Official Newsletter of the International Institute for FRP in Construction

Volume 3, Issue 2 ***Summer 2006***

Welcome to the second issue of the IIFC Newsletter for 2006. As this goes to press activities are ongoing in preparation for CICE to be held this December in Miami. This promises to be a very interesting conference and I look forward to seeing a large number of IIFC members there.

This issue highlights aspects related to rapid bridging and non-destructive evaluation. It also provides an overview of FRP test facilities at the University of California Irvine.

We continue to seek submissions from our readers on new applications of FRP in Construction, forthcoming conferences and workshops, or even general items that may be of interest to the worldwide community. Material can be submitted directly to me at vkarbhari@ucsd.edu or to any of the members on the advisory or editorial boards.

We are planning issues on Structural Health Monitoring, Reliability and Durability – all topics of extreme importance to both the research and commercial communities and would like to invite contributions from our members in these areas as well.

Please also feel free to write to me or to the President of IIFC, Professor J.G. Teng (*cejgteng@polyu.edu.hk*), with any ideas you may have for the newsletter and for IIFC, itself

Vistasp M. Karbhari, Editor-in-Chief
Email: vkarbhari@ucsd.edu

In this issue

FRP INTERNATIONAL

The Official Newsletter of the International Institute for FRP in Construction

Volume 3, Issue 2 Summer 2006

Reports From Around the World

Real-Time and Hand-Held Microwave NDE Technology for Inspection of FRP-Wrapped Concrete Structures

by

Maria Q. Feng[1], Yoo Jin Kim[2] & Kevin Park[2]

[1]University of California, Irvine, CA 92695-2175
[2]Newport Sensors, Inc., Irvine, CA 92612

Many of the nation's bridges, highways, buildings, pipelines and other key structures are deteriorating, falling below capacity, and are in need of immediate repair or replacement (ASCE, 2005). Deployment of high-performance construction materials and systems is essential for successful renewal of the nation's infrastructure. Advanced FRP composites have emerged as a potentially cost-effective alternative to traditional construction materials. They are finding applications wrapping concrete columns and cap beams for strengthening or seismic retrofit, and replacing heavy concrete decks for improved load rating. However, major concerns in long-term performance and durability of FRP composites, and most importantly, the unavailability of effective NDE tools for quality assurance and long-term monitoring, have prevented wide deployment of FRP composites as construction materials. For example, an FRP jacket is often manually applied to a concrete structure member in the filed with adhesive epoxy. The bonding quality between the jacket and the concrete depends largely on the installation workmanship and environmental conditions. Poor bonding, especially the existence of large areas of voids and debonds, can significantly degrade the structural integrity and safety that could otherwise be attainable by FRP jacketing. This has been demonstrated by experiments performed by Haroun et al (1999), in which two reinforced concrete columns with lap splices were wrapped with identical prefabricated glass FRP composite jackets for seismic retrofit: one was well wrapped with the adhesive epoxy carefully applied to the entire jacketing area, while the other was poorly wrapped leaving many voids in the bonding interface.

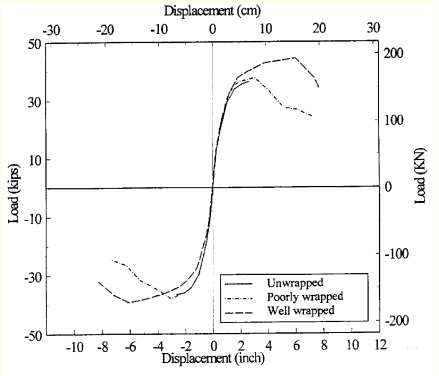

Figure 1. Debonds and Performance Degradation

As shown in Figure 1, the force-displacement envelops resulting from the cyclic loading tests, the well-bonded column performed excellently by increasing the column ductility factor from one (for the unwrapped column) to six, while the poorly bonded column barely reached a ductility factor of three. This testing result demonstrated the needs for NDE inspection of the bonding conditions between the FRP jacket and concrete. The current practice, such as visual inspection, tapping, and sample extraction/testing, is labor intensive, time consuming, destructive to structures, and most importantly, unable to provide sufficient information about the extent of damage.

DESCRIPTION OF MICROWAVE NDE TECHNOLOGY

The microwave NDE technology was developed for detecting invisible defects and damage including, but not limited to, air voids and delaminations inside fiber reinforced polymer (FRP) composites, concrete, and other materials (Feng, et al, 1999, Feng, et al, 2001, Kim, et al, 2003, Kim, et al, 2004). What distinguishes this technology from its peers is its real-time assessment capability and hand portability, as illustrated in Figure 2.

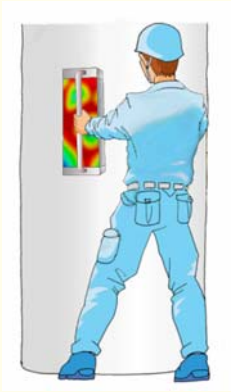

Figure 2. Concept of Real-Time and Hand-Held Microwave NDE Device

Recently, this technology has been commercialized into hand-held products. The device consists of two or several array antennas, a signal source module, and a system controller. The transmitting array antenna focuses a microwave beam onto a point of interest on a structure, and the other array antenna(s) receives the microwave reflected from the structure. Internal defects/damage in the structure can be detected as the antenna system scans the structural surface.

Multiple antenna elements are laid in a matrix format in each of the array antennas. The use of the array antennas enables focusing the microwave into a narrow beam to improve the measurement resolution. A focused microwave beam pattern is illustrated in Figure 3.

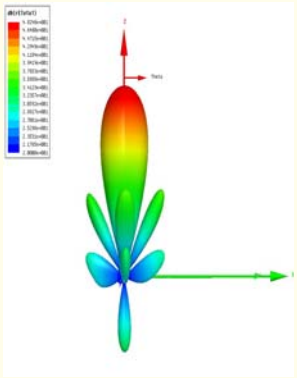

Figure 3. Microwave Beam of Array Antennae

The specific shape of the pattern and size of the beam depends on the number and layout of the antenna elements. Continuous microwaves in the frequency range of 5GHz to 15GHz are used. Optimal frequency is determined based on the required measurement resolution and the depth of inspection of a given material.

There are several different methods to scan a structural surface with the array antennas, including manual scanning, mechanical scanning and electronic scanning by phased arrays.

Defects and damage in a structural subsurface are detected and displayed in a visualized manner, in real time, by analyzing the reflected waves in comparison with a reference measured on the same structure at a location without defects/damage. GAP-CAT-1100, a hand-held all-in-one device, can indicate defects/damage by red and green lights, as shown in Figure 4.

Figure 4. GAP-CAT-1100 Hand-Held All-In-One-Device

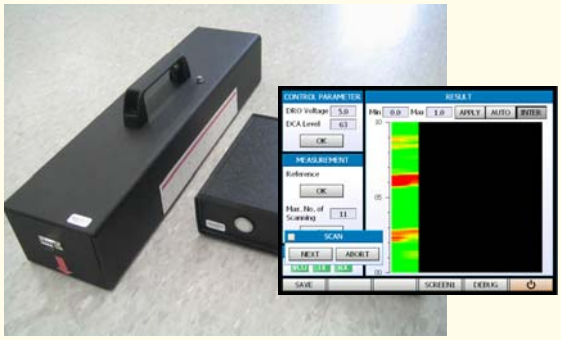

Figure 5. GAP-CAT-1200 With Real-Time Imaging Capability

GAP-CAT-1200, a hand-held scanner, can provide real-time scanned image on a computer screen, as shown in Figure 5. The image can be recorded for long-term monitoring and comparison.

LABORATORY AND FIELD EVALUATION

Extensive laboratory and field tests have been carried out to evaluate the performance of the microwave NDE technology. Emphasis has been placed on detection of delaminations in layered FRP composites and debonds between FRP and concrete.

For the laboratory test, a variety of FRP composites and FRP-wrapped concrete specimens were constructed. Delaminations and debonds were introduced between layers of the FRP composites and in the FRP and concrete bonding interfaces by using Styrofoam inserts (as Styrofoam has the same dielectric property as air). Figures 6 (a) and (b) show the scanned real-time images respectively on an FRP-wrapped concrete block and a seven-layer FRP composites.

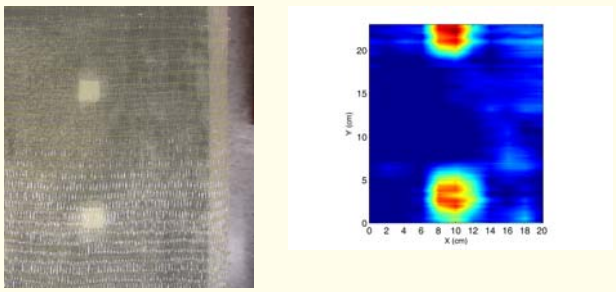

Figure 6(a). Real-Time Image of a Scanned Area on FRP-Wrapped Concrete. The Top Defect is at 1.5 mm Depth and the Bottom Defect is at 1.0 mm Depth

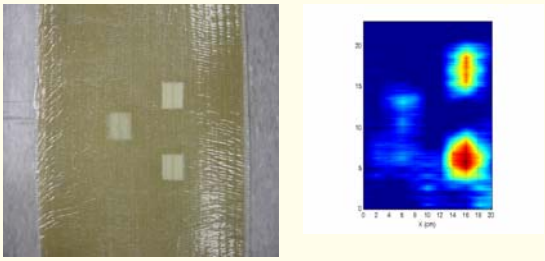

Figure 6(b). Real-Time Image of a Scanned Area on Multilayered Composites. Depths of Defects and Top, Bottom and Left are 1.0 mm, 1.5 mm and 0.5 mm, Respectively

The concrete block is wrapped with two layers of E-glass FRP sheets bonded by adhesive epoxy, and the bonding layer involves two debonds with dimensions of 4 cm x 4 cm x 1.5 mm and 4 cm x 4 cm x 1.0 mm. The seven-layer E-glass FRP composites contain similar debonds between the layers. In both specimens, the debonds were successfully detected and displayed as images in real time.

Additional laboratory tests were performed on prefabricated FRP structural members. Figure 7 shows a successful detection of a change in the member thickness.

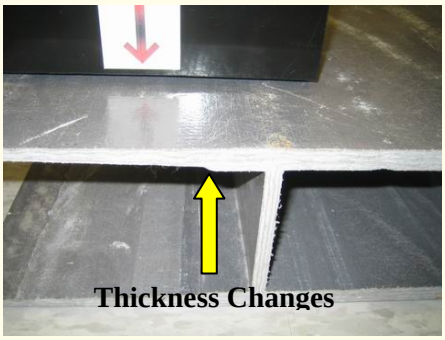

Figure 7. Detection of Thickness Change in FRP Structural Member

So far five major evaluation tests of the microwave NDE technology have been performed in the field. The first two evaluations were carried out at the Caltrans' FRP demonstration site located at I-10, Los Angeles, CA, on May 2 and August 29, 2005, in collaboration with the California Department of Transportation (Caltrans). The site involves concrete bridge columns wrapped with various types of E-glass and carbon FRP jackets for seismic retrofit purposes. Two columns, one wrapped with a 3-layer E-glass prefabricated jacket and the other with a single-layer carbon FRP (hand lay-up) jacket were selected for evaluation (Figure 8). In Column 1, an area of 0.5 m^2 was manually scanned in less than 4 minutes. A debonding area of 5 cm in diameter was detected by the device and later confirmed with manual coin tapping. In Column 2 (with carbon FRP), a debonding area of 3 cm in diameter was detected and later confirmed with coin tapping. Smaller debonds detected by the NDE device could not be verified by manual tapping. Tapping could not quantify the dimensions of the debonds either.

Figure 8(a). Glass FRP Jacketed Columns

Figure 8(b). Carbon FRP jacketed Columns

Figure 9. Field Test at I-80 Yolo Causeway Viaduct in California

A similar evaluation was performed on August 31, 2005 on the I-80 Yolo Causeway Viaduct in Sacramento, CA, where more than two thousand concrete columns were retrofitted with prefabricated FRP jackets. The fourth evaluation test was performed on November 8, 2005 on an FRP-wrapped concrete bridge column in collaboration with the New York State Department of Transportation (NYSDOT). The column, as shown in Figure 10, is located at the south face of a bridge on Congress Street in Albany, NY.

Figure 10(a). E-Glass FRP Wrapped Column

Figure 10(b). Thermography Using Infrared Camera

Figure 10(c). Hand-Held All-In-ONE Microwave NDE Device

It is a 1.2 m by 1.2 m rectangular concrete column wrapped with one layer of hand lay-up E-glass FRP using epoxy resin. NYDOT engineers periodically take thermographs the FRP-wrapped bridge column using a passive-type infrared camera (that does not require pre-heating). The thermograph taken at the column revealed one debonding area that is approximately 0.2 m^2. However, the scanned results over this area by the microwave NDE device indicated four small deponding areas, each with a diameter of 5 cm, instead of one large debonding area. These small debonds were confirmed by manual coin tapping. It was found that the passive thermograph is highly sensitive to environment conditions. It took approximately 3 minutes to scan this 0.2 m^2 area and to mark the four debonds.

The fifth field evaluation took place on March 2, 2006 on an FRP-wrapped concrete girder of the Dang-Jeong Overcrossing located at Gun-Po, Korea. Eight years ago, the bridge girder was retrofitted by Conclinic Co. Ltd. with two layers of E-Glass FRP sheets and external post-tensioning as shown in Figure 11.

Figure 11(a). Inspection of FRP-Wrapped Girders

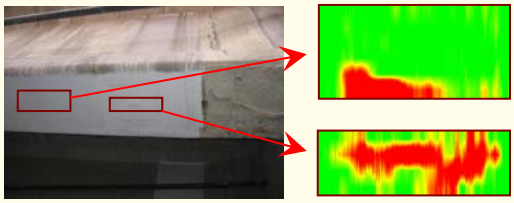

Figure 11(b). Scanned Microwave Images

First, GAP-CAT-1100 (the device with light indicator) was used to pre-scan a large FRP-wrapped girder surface. Although majority of the area showed no sign of debonds (green light), two debonding spots (red light) were identified. Then, more detailed inspection was performed by GAP-CAT-1200, which is capable of providing a real-time image of the scanned area. Figure 11(b) shows the two real-time images revealing the details of the debonding areas. This field evaluation proved the ease of use and the effectiveness of the microwave NDE technology.

CONCLUDING REMARKS

Different from its peers, the microwave NDE technology developed in this research has unique hand-held portability and real-time imaging capability. Extensive field evaluation has demonstrated its user-friendliness and effectiveness in detecting and quantifying delaminations between layered FRP composites and debonds between FRP and concrete. The quantification cannot be achieved by the current manual tapping practice.

ACKNOWLEDGEMENTS

This work was sponsored by the Advanced Technology Program, Department of Commerce. The field evaluation tests would not have been possible without the strong support by Dr. Sreenivas Alampalli at the NYSDOT and Mr. Lihong Sheng at Caltrans. They, together with Dr. Garry Hawkins at the Aerospace Corporation, also provided insightful advice and comments for the technology development. The authors also would like to thank Mr. Ed Fyfe at Fyfe Co. for his useful guidance regarding field implementation issues.

REFERENCES

ASCE (2005), "America's Crumbling Infrastructure Eroding Quality of Life - Report Card Assesses Condition of Nation's Infrastructure".

Feng, M.Q., Liu, C., He, X. and Shinozuka, M. (1999), "Electromagnetic Image Reconstruction for Damage Detection", *Journal of Engineering Mechanics, ASCE*, 126(7), 725-729.

Feng, M.Q., De Flaviis, F. and Kim, Y.J. (2001), "Use of Microwaves for Damage Detection of FRP-Wrapped Concrete Structures", *Journal of Engineering Mechanics, ASCE*, Vol. 128, No. 2, pp. 172-183.

Haroun, M.A., Feng, M.Q., Bhatia, H., Baird, K. and Elsanadedy, H. (1999), "Structural Qualification Testing of Composite-Jacketed Circular and Rectangular Bridge Column", *Technical Report to the California Department of Transportation.*

Kim, Y.J., Jofre L., De Flaviis, F. and Feng, M.Q. (2003), "Microwave tomographic array for damage detection of civil engineering structures", *IEEE Transactions on Antennas and Propagation*, Vol. 51, No. 11.

Kim, Y.J., Jofre, L., Feng, M.Q. and De Flaviis, F. (2004), "Microwave sub-surface imaging technology for damage detection", *Journal of Engineering Mechanics, ASCE*, Vol. 130, No. 7, pp. 858-866.

Monitoring FRP Rehabilitated Bridge Decks

by

Luke Lee[1], Vistasp M. Karbhari[2] & Charles Sikorsky[3]

[1]Louisiana Tech University, College of Engineering and Science, Ruston, Louisiana 71272, USA
Lee@LaTech.edu
[2]Department of Structural Engineering, University of California San Diego, La Jolla, CA 92093, USA
vkarbhari@ucsd.edu
[3]California Department of Transportation, Division of Engineering Services, Sacramento, CA 95816, USA
charles_sikorsky@dot.ca.gov

Many reinforced concrete (RC) structures such as bridges have become structurally and functionally deficient after many years in service due to aging, weathering of materials, accidental damage, increased traffic and industrial needs (Tajlsten 2002; Karbhari and Seible 2000). Since resources do not exist to replace all deficient structures, innovative methodologies and tools are currently being developed to efficiently manage the degradation and structural deficiencies present in existing infrastructure.

For purposes of service life extension, the application of fiber reinforced polymer composites (FRP) to repair and/or strengthen existing bridge structures is increasing. Although significant advantages are realized with FRP composites (i.e. high strength-to-weight ratio, high stiffness-to-weight ratio, ease of construction, tailorability, etc.) questions regarding quality and durability of FRP composites at the material level remain as well as the effect of FRP material degradation on the long-term performance of the rehabilitated component or structure. One potential approach to evaluate the effectiveness of FRP rehabilitated structures has been the implementation of global, vibration based nondestructive evaluation techniques. Implementation of a vibration based NDE approach for condition assessment can assist in determining the long-term performance of FRP rehabilitated structures subject to all conditions, chemical or physical, which contribute to its deficiencies.

This article presents the implementation and results of applying a vibration based monitoring approach to localize and quantify stiffness changes in a RC T-girder bridge structure where the deck slab is rehabilitated with both wet lay-up and pultruded CFRP composites. Results of stiffness changes in the elements (i.e. deck slab and girders) are shown at 1 month, 12 months and 20 months after rehabilitation of the bridge decks. A comparison of the wet lay-up and pultruded rehabilitation shows that the pultruded CFRP composite rehabilitation provided better overall performance in terms of stiffness change.

BRIDGE DESCRIPTION

The Watson Wash Bridge is a skewed RC T-girder bridge located on California Interstate 40 in the Mojave Desert and was constructed in 1969. Figure 1 provides an overview of the spans and bays of the bridge structure.

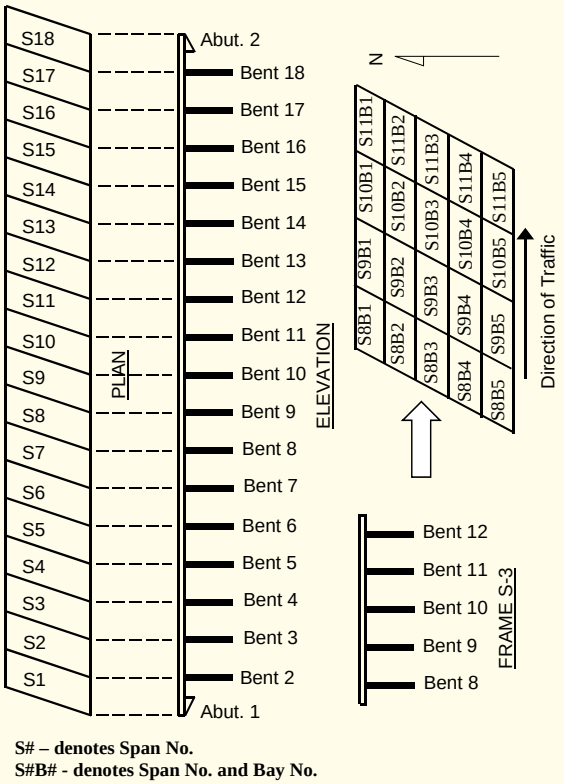

Figure 1. Overview of Watson Wash Bridge and Frame S-3

The superstructure consists of a cast-in-place reinforced concrete deck and girder structural system with sixteen 12.8 m central spans and two shorter spans of 10.52 m at each abutment. The 156 mm thick deck spans transversely across six girders at 2.13 m centers. The bridge is built of 18 spans and five bays within each span. The bridge is composed of five frames connected with shear transfer hinges. The T-girders are 762 mm deep from top of the deck to the base of the girder, with a girder width of 280 mm. The effective deck slab width is 1854 mm. All monitoring and rehabilitation activities are conducted in the center frame, Frame S-3, composed of spans 8 through 12 as shown in Figure 1. Bays within each span are identified 1 thru 5 from North to South, i.e. bay 3 of span 9 is denoted S9B3.

CHARACTERISTIC DAMAGE

A visual inspection of the Watson Wash Bridge reveals a significant number of transverse cracks in the soffit of the bridge deck. The spacing of these cracks is approximately 14 cm corresponding to the average spacing of the transverse reinforcement in the deck of the bridge. Transverse and longitudinal cracking exist near the center of bay 4 of Frame S-3 which corresponds to the right wheel load of east bound traffic on the right lane of I-40 of the Watson Wash Bridge. The evenly spaced cracking in both directions on the bridge soffit indicates the potential for punching shear failures. Figure 2 shows the longitudinal and transverse crack patterns on the bridge deck. The sequence of damage observed on the structure is as follows. First, the development of transverse cracks effectively reduces the slab to a series of transverse beams normal to the direction of traffic. Subsequently, longitudinal cracks develop on the bridge deck soffit creating the potential for punching shear failure in the deck slab.

Figure 2. Transverse and Longitudinal Cracking on Bridge Deck

FRP REHABILITATION

The damage assessment revealed that development of transverse and subsequent longitudinal cracking is due to increased load demands on the bridge structure and the lack of steel reinforcement to accommodate increased loads. Steel reinforcement deficiencies in the slab are calculated by analyzing the existing structure with respect to current code requirements and for prevention of punching shear failure. A summary of the computed steel reinforcement area deficiencies per meter of slab width are provided in the table below with respect to the load condition (Lee 2005).

Table 1. Summary of Reinforcement Deficiencies in cm^2/m

Reinf. Direction	Load Condition		
	HS20-44 Truck	Permit Truck	Punching Shear
Transverse	1.06	7.62	--
Longitudinal	0.66	3.81	2.94

Utilizing computed steel reinforcement deficiencies; an equivalent CFRP rehabilitation design is determined based on the stiffness of the composite material and a maximum strain limit of 0.75% to ensure sufficient aggregate interlock (Lee et al. 2005). The number of CFRP composite strips corresponding to the steel reinforcement deficiencies is determined for rehabilitations constructed via wet lay-up of carbon fabric strips and adhesive bonding of pultruded CFRP composite strips. Details of the CFRP composite rehabilitation design are available in (Lee 2005). As an example, the CFRP rehabilitation design for the punching shear load condition using the wet lay-up and pultruded strips is provided in Table 2.

Table 2. Summary of Rehabilitation Design for Punching Shear Load (# of Strips)

Direction	Wet Lay-up	Pultruded
Transverse	21, two layers	21
Longitudinal	4, one layer	4

Completed rehabilitations are shown in Figure 3 for wet lay-up and pultruded CFRP composites.

Figure 3. Completed Rehabilitation, Adhesive Bonding (Left) and Wet Lay-up (Right)

The minimum requirement for the deck rehabilitation is prevention of punching shear failure. Locations span 8, bay 1 (S8B1), S9B1, and S9B4 are rehabilitated with pultruded CFRP composites for the punching shear load criterion. Locations S8B2, S8B3, S9B2, and S9B3 are rehabilitated considering the Permit truckload requirement, 106.8 KN (24 kips), with wet lay-up CFRP in S8B3, S9B3 and pultruded CFRP in S8B2, S9B2. Location S8B4 is left unrehabilitated for purposes of comparison.

MONITORING

As part of the monitoring process, a global vibration based NDE of the rehabilitated bridge structure is conducted. The methodology localizes changes in a structure from its global response for a specified interval of time. Monitoring of the structure involves: (1) modal testing of the bridge structure; (2) modal parameter extraction to acquire modeshapes and frequencies; (3) a vibration based NDE algorithm to quantify structural changes from changes in modal parameters. The results for monitoring of the Watson Wash Bridge structure at 1 month, 12 months, and 20 months after rehabilitation are provided.

MEASUREMENT OF DYNAMIC PROPERTIES

The objective of the modal test is to implement an experimental procedure to acquire acceleration time histories at different points and directions of a structure, in order to ascertain the modal model through experimental modal analysis. During each of the modal tests, normal traffic over the bridge structure was used as the source of ambient vibration. Ambient excitation using normal traffic was selected for the following reasons: (1) Use of ambient vibration does not require closure of the bridge structure or interruption to bridge service; (2) Use of normal traffic excitation illustrates potential for autonomous health monitoring of large scale bridge structures. Acceleration time histories were measured using standard capacitive accelerometers, attached to the soffit of the RC bridge structure with aluminum mounting plates. Details of modal testing, sensor configurations and spacing are available in (Lee 2004).

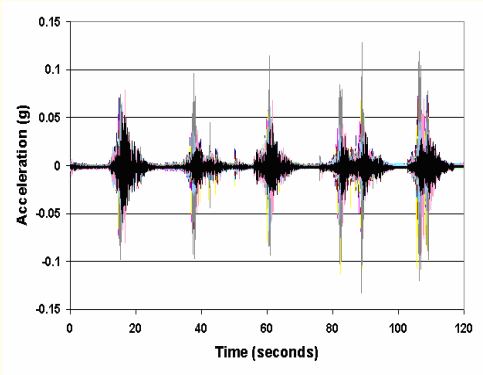

Figure 4. Typical Measured Acceleration Time History Data

Figure 4 shows a representative sample of acceleration time history data recorded from the bridge structure. As normal traffic traverses the bridge structure, acceleration data is recorded at 200 samples/sec at each sensor location. From the measured acceleration time history, an output only modal analysis procedure referred to as time domain decomposition (TDD) (Kim 2002) is used to extract modeshapes of the bridge structure. An example of an extracted modeshape is shown in Figure 5. Modal properties of the bridge structure were measured before, one month after, 12 months after, and 20 months after rehabilitation.

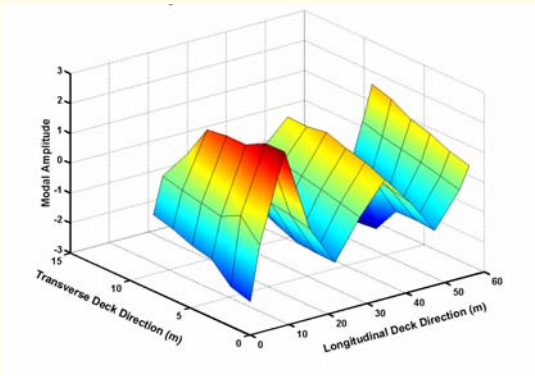

Figure 5. First Bending Mode, 12 months After Rehabilitation

VIBRATION BASED NDE

Output only modal testing and experimental modal analysis represents the data collection component of the structural health monitoring process. The nondestructive evaluation process requires the use of a damage detection algorithm to identify stiffness changes in a structure. For the purposes of this analysis, the damage index method by Stubbs et al. (2000) is applied to detect changes in modal strain energy. The damage index is denoted by the following formulation.

$$\beta_j = \frac{k_j}{k_j^*} = \frac{1}{2}\left[\frac{\Phi_i^{*T} C_{j0} \Phi_i^*}{\Phi_i^{*T} C^* \Phi_i^*} \cdot \frac{\Phi_i^T C\ \Phi_i}{\Phi_i^T C_{j0} \Phi_i} + 1\right] \tag{1}$$

where k_j, and k_j* are scalar parameters representing the material stiffness properties of the undamaged and damaged j^{th} member of the structure; C_{j0} is a matrix of geometric quantities (and possibly terms containing Poisson's ratio); C and C* are the system stiffness matrices for the undamaged and damaged structure; Φ_i and Φ_i^* are the respective undamaged and damaged i^{th} modal vectors. If β_j is greater than one, damage may exist; if β_j is less than one and greater than zero, a stiffness increase may have occurred.

The severity estimation in terms of fractional stiffness loss or increase, α_j, is given for each potentially changed element, j, by equation (2).

$$\alpha_j = \frac{k_j^* - k_j}{k_j} = \frac{1}{\beta_j} - 1 \tag{2}$$

where β_j is the damage index shown in equation (1). All other variables are defined previously. If $\beta_j > 1$, a stiffness loss in element j has occurred; $\beta_j < 1$ indicates a stiffness increase in element j; and $\beta_j = 1$ indicates no stiffness change in element j. The procedure is applied according to the following steps:

a) Calculate mode shape curvatures using a cubic spline curve fit of the mode shape and numerical derivatives (computations were conducted using commercial programming languages such as in Matlab).
b) Calculate the damage index, β_j, for each element, j.
c) The fractional stiffness change, α_j, (loss or gain) is determined. If $\alpha_j > 0$, then an increase in stiffness has occurred; if $\alpha_j < 0$, then a loss in stiffness is deemed to have occurred.

DAMAGE INDEX RESULTS

The damage indicator results are used to identify locations where increases or decreases in stiffness have occurred during normal service of the structure. For the monitoring of spans 8, 9, 10 and 11 of the Watson Wash Bridge, the structure is divided into 20 elements. Each element represents an area of the deck slab between girders and the adjacent girders in each span. Figure 1 shows the elements representing the deck slab of the bridge. One element represents a single bay of the Watson Wash Bridge. Of these elements, those that are rehabilitated with CFRP composites are denoted in white and identified by composite manufacturing technique; locations that are not rehabilitated are denoted in gray. Each element is identified by its span and bay location, i.e. span 9, bay 5 is element S9B5.

Figure 6 shows damage index results from comparing modal strain energy before and after rehabilitation of spans 8 and 9 with CFRP composites. The white bars denote rehabilitated locations, whereas gray bars are non-rehabilitated locations. A damage index value, β_j, less than one indicates that stiffness has increased in a bay of the bridge deck; a β_j value greater than one indicates that a decrease in stiffness in the bay of the bridge deck has occurred. In Figure 6, damage index values less than one are measured in spans 8 and 9 as expected since CFRP composite rehabilitations are constructed in those locations. A damage index value less than one in S8B4, a non-rehabilitated location, is attributed to the stiffening effects in adjacent locations. In the non-rehabilitated locations of spans 10 and 11, damage index values greater than one are observed, indicating stiffness losses in the region.

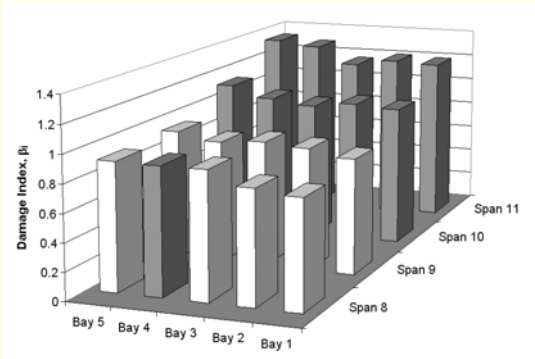

Figure 6. Damage Indices 1 month After Rehabilitation

Figure 7 shows damage index results evaluating changes in modal strain energy at 12 months after rehabilitation.

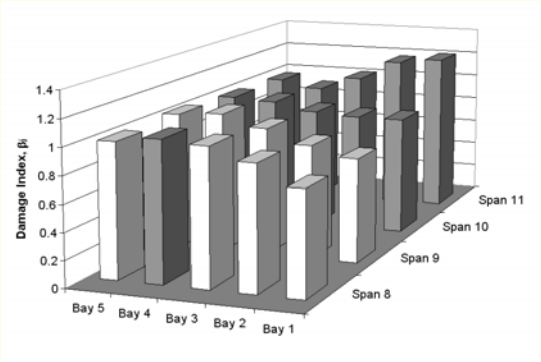

Figure 7. Damage Indices 12 months after Rehabilitation

In bays 3, 4, and 5 of spans 8 thru 12, a uniform distribution of damage index values is observed, which suggest that stiffness redistribution occurs in the right lane of traffic where heavier truck loads are observed. Bays 3 and 5 of spans 8 and 9 correspond to regions surrounding the non-rehabilitated location of S8B4, as well as wet lay-up manufactured CFRP composites.

In bays 1 and 2 of spans 8 thru 11, the damage index results show a similar pattern as compared to Figure 5. The pultruded CFRP rehabilitated locations, S8B1, S8B2, S9B1, and S9B2 continue to show damage index values less than one, indicating the stiffness increase is maintained at 12 months. Whereas wet lay-up manufactured locations, in S8B3, S8B5, S9B3, and S9B5 are not performing as well.

Figure 8 shows damage index results evaluating changes in modal strain energy at 20 months after rehabilitation. Bays 3, 4 and 5 of spans 8 thru 11 are generally performing at the same damage index level as was measured at 12 months, except a general increase in the damage index is noted in span 11. The pultruded CFRP rehabilitation in bays 1 and 2 of spans 8 and 9 continue to indicate a general stiffness increase due to rehabilitation at 20 months.

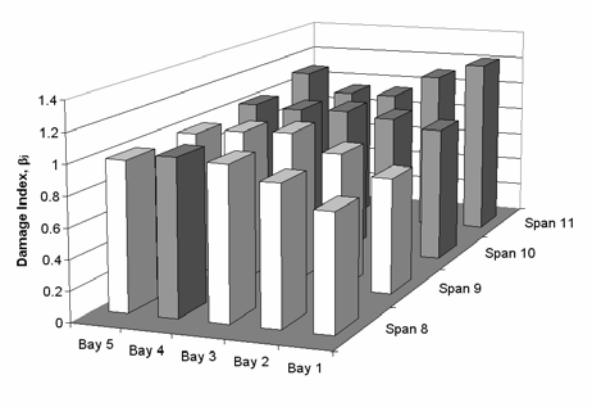

Figure 8. Damage Indices 20 months after Rehabilitation

STIFFNESS CHANGES

The damage indicator estimates changes in modal strain energy comparing a reference state (i.e. mode shape prior to rehabilitation) to another state of the structure (i.e. mode shape at time t = 12 months). By applying equation (2) to the calculated damage indices, fractional stiffness losses, α_j, are determined for each bay of the bridge structure. Use of this procedure immediately after rehabilitation shows an average stiffness increase of 16.63% in span 8 and 13.10% in span 9, which correspond to the rehabilitated spans of the bridge. In spans 10 and 11, average stiffness losses of –3.48% and –19.64% are calculated, respectively, corresponding to the unrehabilitated spans of the bridge structure. All bays of span 8 show increases in stiffness with the greatest increase occurring in location S8B1 at 28.77% for a pultruded CFRP rehabilitation. The lowest stiffness increase is observed in S8B5 at 9.77% for a wet lay-up rehabilitation. It is important to note that location S8B4 is unrehabiltiated and its stiffness increase is attributed to the stiffening provided by adjacent bays of the bridge structure. In span 9, the highest stiffness increase occurs in bay 1, a pultruded CFRP rehabilitated location. The lowest stiffness increase of span 9 is measured in S9B5 at 7.27%. As expected the rehabilitated regions of spans 8 and 9 show increased levels of stiffness after construction of the CFRP composites. In general the pultruded CFRP composite rehabilitations of bays 1 and 2 indicate greater levels of fractional stiffness change than wet lay-up repaired regions.

12 months after rehabilitation with CFRP composites, it is noted that average stiffness increases of 6.18% and 8.7% are calculated for spans 8 and 9 respectively. In bays 3, 4 and 5 of spans 8 and 9, corresponding to wet lay-up construction, a decrease in stiffness is observed that indicates those bays (i.e., deck and adjacent girders) returned to a stiffness level similar to levels prior to rehabilitation. This may attributed to weakening of adjacent girders as a result of stiffening in the deck slab. It is also important to note that bays 3, 4 and 5 correspond to the right lane of vehicular traffic where heavier truck loads are observed. As deterioration in spans 8 and 9 occurs, a stiffness redistribution of the structure is observed in spans 10 and 11 for bays 3, 4 and 5. The pultruded CFRP composites applied in bays 1 and 2 of spans 8 and 9 continue to indicate increases in stiffness; however, the fractional stiffness change in span 8, bay 2 has decreased from 23.71% (1 month after rehabilitation) to 8.07% (12 months after rehabilitation).

20 months after rehabilitation with CFRP composites average stiffness increases of 7.26% and 7.55% are calculated for spans 8 and 9 respectively. The performance of wet lay-up composite locations in bays 3, and 5 of spans 8 and 9, continue to remain at approximately the same stiffness levels as measured at 12 months. For the pultruded CFRP rehabilitation locations, bay 1 of spans 8 and 9 continues to show a high level of stiffness increase (~30%) at 20 months after the rehabilitation; whereas bay 2 of spans 8 and 9 show stiffness increases of 8.7% and 9.95% at 20 months after rehabilitation.

Plotting stiffness changes with respect to time for each inspection stage, shows the time dependent performance of each bay (i.e. deck slab and adjacent girders) relative to one another. Figures 9 and 10 are graphs of stiffness changes in spans 8 and 9 after rehabilitation with CFRP composites.

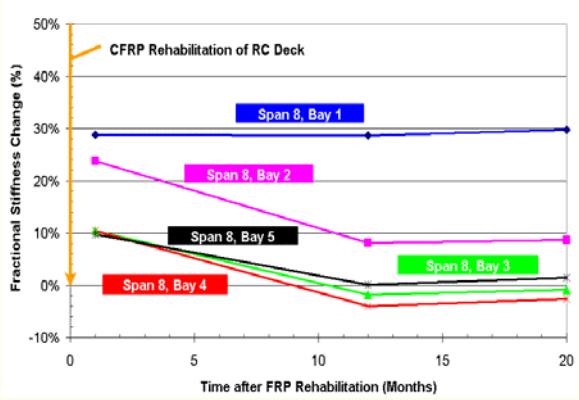

Figure 9. Stiffness Changes in Span 8 After Rehabilitation

Figure 9 shows stiffness changes in the bays of span 8 at 1 month, 12 months, and 20 months after rehabilitation. Only the pultruded CFRP rehabilitation in bays 1 and 2 indicate a stiffness increase at 20 months after rehabilitation, while the wet lay-up CFRP rehabilitations of bays 3 and 5 show stiffness levels returning to the condition of the bay prior to rehabilitation. The decrease in fractional stiffness change may be due to weakening of girders as a result of stiffening of the adjacent deck slabs with CFRP composites.

Figure 10 shows stiffness changes of span 9 at 1 month, 12 months, and 20 months after rehabilitation. Again, the pultruded CFRP rehabilitation in bays 1 and 2 is shown to have a better overall performance than wet lay-up repaired deck slabs. While stiffness levels in the wet lay-up CFRP repaired regions in bays 3 and 5, tend to return to its pre rehabilitation state at 12 months and 20 months after rehabilitation. This decrease in stiffness levels may be associated with the weakening of girders as a result of stiffening in the adjacent slabs due to increased load transfer.

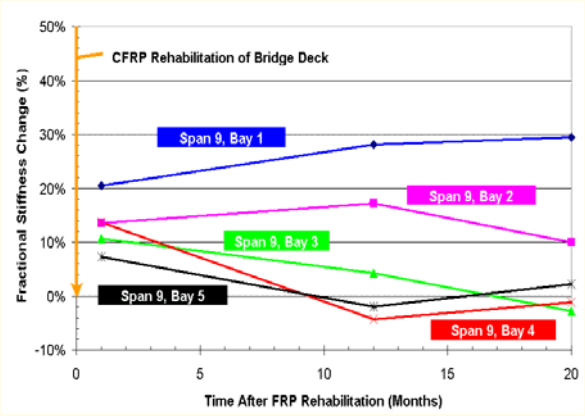

Figure 10. Stiffness Changes in Span 9 After Rehabilitation

CONCLUSIONS

By employing a vibration based damage detection procedure an assessment of the FRP composite bonded to the deck soffit of spans 8 and 9 of the Watson Wash Bridge was conducted. A global vibration based NDE approach measuring changes in modal strain energy was applied to determine fractional stiffness changes of the RC T-girder structure at specified intervals. Application of a monitoring approach is one means to assess the performance of a field rehabilitation with respect to time.

REFERENCES

Karbhari, V.M. and Seible, F. (2000), "Fiber Reinforced Composites - Advanced Materials for the Renewal of Civil Infrastructure", *Applied Composite Materials*, 7, 95-124.

Kim, B-H. (2002), "Local Damage Detection Using Modal Flexibility" *PhD Dissertation, Civil Engineering, Texas A&M University.*

Lee, L.S. (2005), "Monitoring and Service Life Estimation of Reinforced Concrete Bridge Decks Rehabilitated with Externally Bonded Carbon Fiber Reinforced Polymer (CFRP) Composites", *PhD Dissertation, Structural Engineering, University of California, San Diego*, 275 pages.

Lee, L.S., Karbhari, V.M. and Sikorsky, C. (2004), "Investigation of Integrity and Effectiveness of RC Bridge Deck Rehabilitation with CFRP Composites", *Structural Systems Research Project Report No. 2004/08, Department of Structural Engineering, University of California, San Diego, September 2004.*

Stubbs, N., Park, S., Sikorsky, C. and Choi, S. (2000), "A Global Non-destructive Damage Assessment Methodology for Civil Engineering Structures", *Intl. J. Systems Science*, 31(11), 1361-1373.

Tajlsten, B. (2002), "FRP Strengthening of Existing Concrete Structures – Design Guidelines", *Lulea University Printing Office, Lulea, Sweden.*

Virtual Testing and Progressive Failure Analysis of Army Composite Bridge

by

Ayman Mosallam[1], Frank Abdi[2], Rashid Miraj[2] & Jian-Juei Wang[3]

[1]University of California at Irvine, Irvine, CA, USA
mosallam@uci.edu
[2]Alpha Star Corporation, Long Beach, CA, USA
[3]The Boeing Company, Huntington Beach, CA, USA

In the recent years, the use of advanced composites in building bridges and bridge components for both civilian and military applications became an attractive topic of research for many structural engineers (1, 2, and 7). Composite bridges provide several attractive features including its lightweight (*high strength-to-weight ratio*), as compared to comparable steel and aluminum bridges, as well as its superior corrosion resistance properties that is preferred in harsh environmental conditions. The lightweight features of composite is an attractive and essential property in order to fulfill the goal of the US army in producing lighter bridging components that require less skill/craftsmanship to manufacture, requires less equipment and manpower to transport and repair as well as being cost effective in the long run. However, during hostile battlefield conditions, damages are likely to occur due to a variety of reasons including punctures from rocks, impact loads from deployment/handling, dropping the structure from moderate heights and various battlefield threats (3). There is an urgent need to develop reliable field repair techniques to ensure the continuity of mission operational capabilities of the composite bridge in case the occurrence of localized damages of different elements of the bridge.

In order to develop an effective repair methodology for military composite bridges, and in order to verify its validity through virtual testing, one should identify i) the most potential loading scenarios that would cause damages to the bridge including extreme live loading conditions, and ii) loads that the "repaired" bridge should withstand after being repaired. The information presented in this paper covers the first loading set. The first part of this study involved calibrating the materials constituent properties of the composite army bridge that will be used in demonstrating and virtually verifying the smart repair technology for military bridges. In the second part of the study, GENOA virtual testing and progressive failure simulations were performed on the composite treadway under three different loading cases. The three cases used in this study are: i) Maximum static shear loading case (Load Case 1), ii) Maximum static moment loading case and iii) fatigue progressive failure analysis for the maximum moment case loading (Load Case 2).

CALIBRATION OF MATERIALS CONSTITUENT PROPERTIES USING GENOA MCA AND PFA CODES

The objective of this analysis is to calibrate the materials constituent properties of the composite army bridge that will be used in demonstrating and virtually verifying the smart repair technology for army bridges. This calibration process is essential in developing both the NASTRAN finite element (FE) and the GENOA Progressive Failure Analytical (PFA) models of the composite army bridge before and after damage as well as after performing the smart repair process.

In order to gain confidence in the material properties that will be used in evaluating the field repair methodology and to ensure reliable results, calibration of materials constituent properties that include weighing the effect of the braided tri-axial properties was preformed.

Material calibration is a back calculation process of constituent properties based on the lamina test data. The purpose of this calibration process is to build a databank to be used in for structural analysis of the bridge structure. In addition, material calibration is necessary because lamina and laminate manufacturing involves many unknowns and variables that influence product properties. The use of mechanical properties supplied by vendors usually results in overestimating both the lamina and laminate properties. The numerical material calibration is similar to the concept of coupon tests (virtual testing).

In this process, the GENOA code is used to calculate the mechanical properties of each ply using best available constituent data (e.g. fibers, matrix, etc). If the calculated ply properties do not match the experimental data, then the constituent properties are adjusted until the experiments and predictions are in agreement. It should be noted that ply properties are calculated from algebraic equations that are functions of the constituent properties. For a single set of fiber and matrix properties, there are almost 50 different values that can be changed in order for each of the ply properties to match any available data; fortunately, each of the ply properties only depends on about 2 to 10 different constituent properties, and is highly sensitive to only a few of those constituent properties. Therefore, in trying to match up each ply property at a time, only two or three variables are manipulated between each prediction. Because the calibration process is performed by calculating ply properties, comparing them to experimental results, manipulating the constituent properties if needed, and repeating the process until predictions match experimental results, a step back must be taken to correct what seems to be the case at first glance. It should be noted that the data analyzed during the calibration process should not be viewed as two separate "measurements" - the predictions and the experiments, that are parallel to each other yet must end up with the same result. First, it should be assumed that the experimental results are reliable and are measured from a ply whose constituent properties were not measured at the time of the experiment. The rest of the calibration process/prediction match up occurs in series. The experimental results are then set equal to the same results that would be obtained from a mathematical, mechanics of materials model of the ply of concern. Finally, the fiber and matrix properties that would give similar mathematical results are then sought. This becomes a root finding problem, not a curve fitting process, for each of the ply properties. At some point in the design space for each ply property, the prediction will match the experiment. Calculating ply properties using mathematical models of composite materials and these inputs and having the values match up to experiments is a good accomplishment. It states that a set of fiber and matrix properties, or design point, has been found that could possibly be the same set of properties that might have been measured from the plies tested experimentally.

The following are the typical procedure used in the calibration process:

1. Prepare a databank with fiber/matrix properties as close as possible to the calibrated fiber/matrix properties. The closer, the faster the calibration process will be. Or use the fiber/matrix properties from vendors.
2. Understand the dependency of lamina properties on constituent properties using the sensitivity module in GENOA-MUA (The detailed steps for running GENOA-MUA are given in Appendix A).
3. Using GENOA-MCA, adjust fiber/matrix moduli in the databank until the calibrated lamina moduli agree with the lamina test data.
4. Adjust fiber/matrix strengths in the databank until the calibrated lamina strengths agree with the lamina test data.
5. If the composite laminate coupon test data is available, simulation may be conducted for further confirmation of the calibrated databank using GENOA-PFA.

Steps 2 and 3 can be switched because the calibrations of lamina moduli and strengths are not obviously coupled. Figure 1 shows the flowchart of the GENOA calibration procedure.

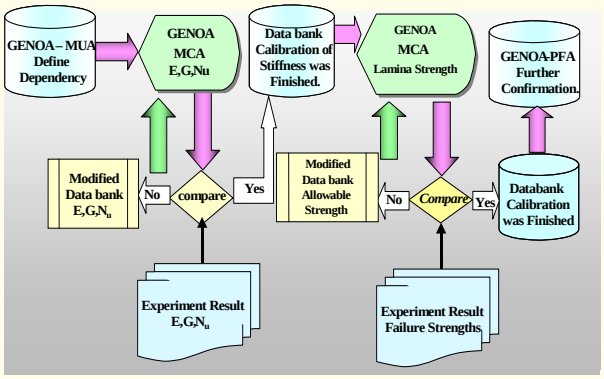

Figure 1. The Genoa Calibration Procedure

A total of four different composite materials were calibrated in this task that comprise the structure of the army composite bridge (refer to Figure 2). Prior to performing the calibration process, original mechanical information was identified from Ref [1].

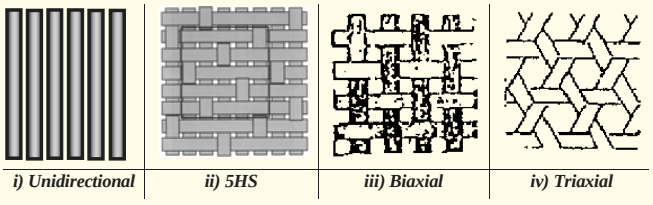

Figure 2. Types and Geometry of Fibers Used in the FEM Analysis

The results of the calibration process identified several variations, especially in the shear moduli, strength and Poisson's ratios. As expected, the original and the calibrated results for unidirectional laminates agreed well. Table 1 presents a summary of the calibration results that includes the effect of kinking of the braided laminates. Figures 3 through 6 present graphical presentation of the results obtained from the calibration analysis for different materials.

Table 1. Summary of Calibration Results*

No Kinking	*Kinking*	*No Kinking*	*Kinking*	*No Kinking*	*Kinking*
6.85	6.53	5.57	5.28	1.91	1.79
6.85	6.02	2.2	2	1.91	1.79
0.416	0.39	2.44	2.2	4.86	4.38
0.374	0.35	0.402	0.39	0.494	0.49
0.374	0.36	0.3747	0.36	0.494	0.49
0.0313	0.034	0.77	0.76	0.83	0.82
0.617	0.6395	0.18	0.20	0.106	0.1163
0.617	0.6502	0.41	0.44	0.106	0.1163
88.3	93.7	54.5	57.9	23.4	23.4
55	57.1	35	35.6	24	24
88.3	84.9	12.6	13.7	23.4	23.4
55	52.8	18.4	18.4	24	24

** The unidirectional results are not included in this table since the calibrated and the original properties were in good agreement (refer to Figure 3).*

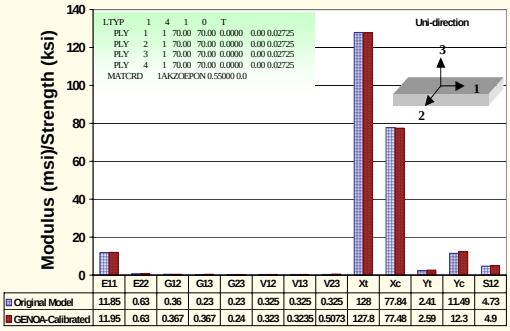

Figure 3. A Comparison between Calibrated and Original Mechanical Properties of Unidirectional Laminates

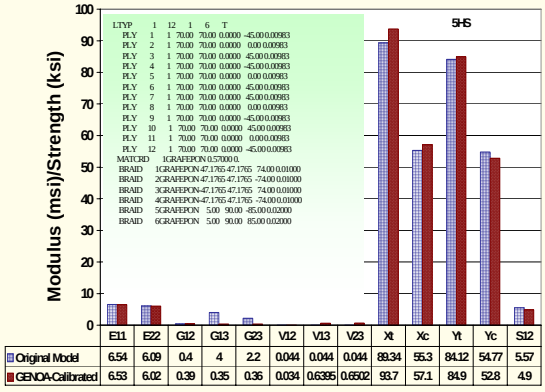

Figure 4. A Comparison between Calibrated and Original Mechanical Properties of 5HS Laminates

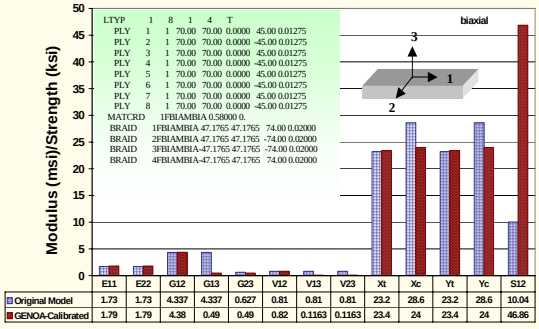

Figure 5. A Comparison between Calibrated and Original Mechanical Properties of the ±45° Biaxial Laminates

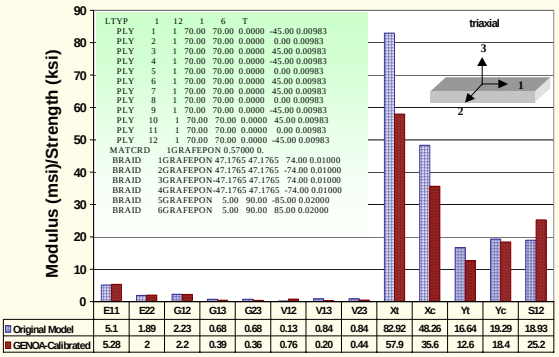

Figure 6. A Comparison between Calibrated and Original Mechanical Properties of the Triaxial Laminates

PROGRESSIVE FAILURE ANALYSIS

The maximum shear loading case (*Load Case 1*) and the maximum bending loading case for MLC 100 described in Ref. [1] were simulated using the GENOA code. In addition, a fatigue progressive failure analysis was conducted for the maximum moment case loading (Load Case 2).

Load Case 1 (Maximum Shear)

The NASTRAN FEM model of the composite bridge treadway was transformed into a GENOA numerical model. The model consisted of 14,514 mixed elements. A Progressive Failure Analysis (PFA) was performed on this model for Load Case 1 (Max Shear) shown in Figure 7. Unlike the NASTRAN FEA, the GENOA analysis is non-linear. Any damage or fracture calculated to have occurred in the structure causes the model stiffnesses to change and the internal loads to redistribute.

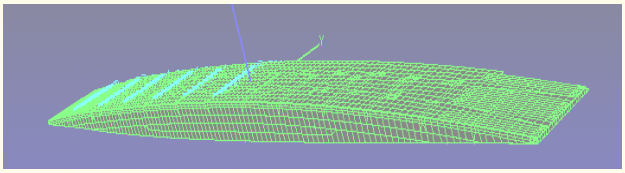

Figure 7. Static Shear Loading Pattern (Load Case 1)

Larger deflections would, therefore, result. In the case of the CAB model, some damage occurs at the working pressure level. In GENOA parlance, damage and fracture failure are distinctly different phenomena. Damage is defined as an intra-lamina event. One or more plies in a laminate have failed. The laminate still has a load bearing capacity albeit at a lower level. The laminate properties are reduced for subsequent GENOA analyses. Fracture occurs in GENOA when laminate level failure has been reached at a node. The GENOA model is modified at a fractured node by disconnecting it from adjacent, non-fractured elements. This also results in an altered load path. When the accumulation of damage and fracture causes the structure's load bearing capacity to drop to zero, it is considered to have failed.

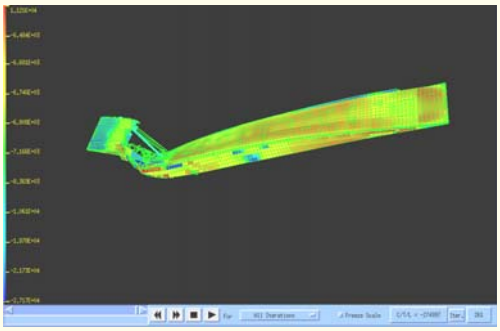

Figure 8. Generalized N_{xy} (lb-in) Shear Stress Distribution at the Ultimate Load [280 kips (1,245.44 kN)]

The maximum deflection at the service load was 3.31" (84 mm) as compared to 3.42" (86.86 mm) experimental value reported in Ref. [1]. The variation between the experimental and GENOA predicted maximum displacement was 3.4%. The ultimate failure was a combination of local damage of both the balsa wood and the composite sidewalls of the bridge (refer to Figure 8). A summary of both experimental and simulated results for the maximum shear loading case is shown in Table 2.

Table 2. Summary of Experimental and PFA Results for Load Case 1 (Max Shear)

Experimental Service Load	151 kips (672 kN)
GENOA Ultimate Load	280 kips (1,245.5 kN)
Experimental Ultimate Load	Not Available
Maximum Displacement at Service Load (GENOA)	3.31 inches (84.10 mm)
Maximum Displacement at Service Load (Experimental)	3.42 inches (86.87 mm)
Maximum Displacement at Ultimate Load (GENOA)	6.26 inches (159 mm)
Maximum Displacement at Ultimate Load (Experimental)	Not Available

Load Case 2: Maximum Moment

Similar to Load Case 1, the NASTRAN FEM model was transformed into a GENOA numerical model. A progressive failure analysis (PFA) using GENOA simulation code was performed on the bridge model for Load Case 2 (Max Shear) shown in Figure 9 which is identical to the loading pattern used in the large-scale laboratory tests performed and described in Ref. [1].

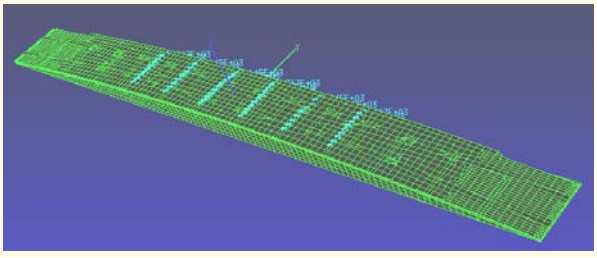

Figure 9. Static Flexural Loading Pattern (Load Case 2)

The GENOA-PFA simulation was initiated at a single actuator load level of 107 kips (476 kN). At this initial loading, no fractured nodes were formed. However, a total of 105 local damages were calculated. Although, no fractured nodes were observed, the number of local ply damages was increased (refer to Figure 10).

The last equilibrium was achieved at a load level of 202 kips/898.50 kN per loading actuator which was set to be the ultimate failure load. At this load level, a total of 11 nodes were fractured resulting in ultimate failure of the bridge. The node damage distribution just before the ultimate failure is shown in Figure 10.

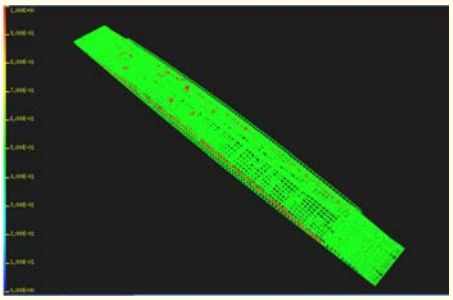

Figure 10. Nodes Damage Distribution at Initial Loading Level

As mentioned earlier, the majority of the local damages were concentrated at the span mid third at both the deck balsa wood and the composite sidewalls as shown in Figure 11.

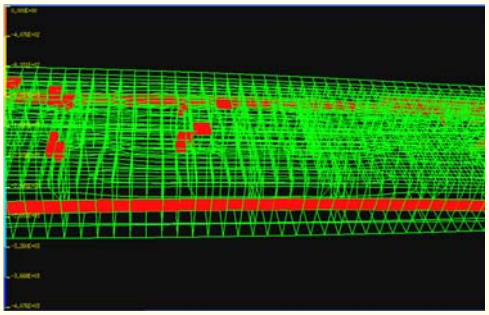

Figure 11. Zoom-In Top View of Damage Distribution Just before the Ultimate Failure

The concentration of these localized damages led to the ultimate failure of the bridge treadway as shown in Figure 12. The location and mode of simulated failure were close to those observed in the laboratory test that was reported in Ref. [1]. The simulated maximum displacement at failure was 6.87 inches (174.50 mm) as compared to 6.80 inches (172.72 mm) as reported in Figure 142 of Ref. [1]. A comparison between the simulated and experimental actuators loads are presented in Figure 13.

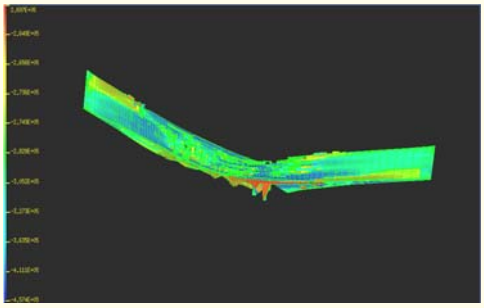

Figure 12. Ultimate Failure of the Composite Bridge Treadway

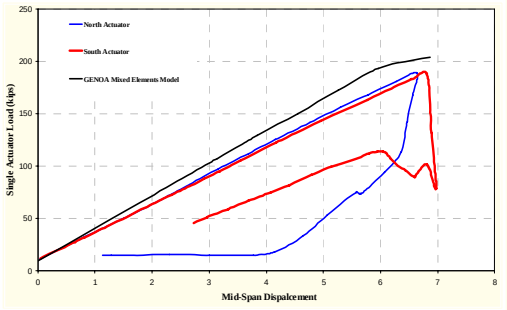

Figure 13. Comparison between Full-Scale Experimental and GENOA Predicted Results for Load Case 2 (Max Moment)

Progressive Fatigue Failure Analysis

The GENOA computational simulation is implemented by the integration of three distinct computer codes that are used as the modules of a progressive fracture tracking code. These computational modules are: (1) composite mechanics, (2) finite element analysis, and (3) damage progression tracking. The overall evaluation of composite structural durability is carried out in the damage progression module that keeps track of composite degradation for the entire structure. The damage progression module relies on a composite mechanics code [Ref. 4] for composite micromechanics, macromechanics, laminate analysis, as well as cyclic loading durability analysis, and calls a finite element analysis module that uses anisotropic thick shell and 3-D solid elements to model laminated composites [Ref. 5].

The composite bridge treadway was subjected to a cyclic loading up to failure. The fatigue analysis was performed to maximum moment load case (Case 1) as shown in Figure 9. The GENOA-PFA simulation started at 5,000 cycles and was continued until the failure occurred. As mentioned earlier, a degradation factor of 0.1 was used in constructing the assumed S-N relation with a stress ratio (R) equal to zero.

After 7,500 cycles another two nodes were fractured. Another node was fractured at the end of the 11,250 cycles with accumulative number of fractured nodes of five. As the number of cycles increased, the number of fractured were increased, especially at the 25,312 cycle where a total of 7 nodes were fractured during this loading cycle in addition to the 5 fractured nodes formed during the earlier cycles. The last equilibrium prior of the ultimate failure was achieved after 128,140 cycles, which was set to be the fatigue life of the composite treadway. Figures 14 and 15 show the generalized N_x (lb-in) stress distributions after 128,140 cycles. The damage growth was monitored using the modified-distortion-energy-damage criteria.

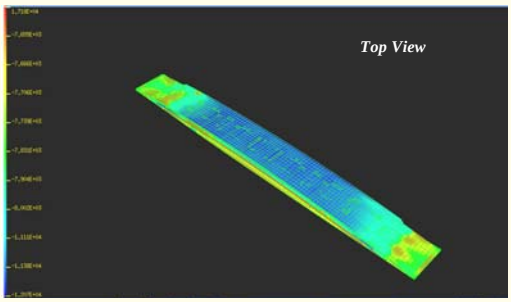

Figure 14. Generalized Normal Stress N_x (lb-in) Distribution after 128,140 Cycles (Fatigue Life) – Top View

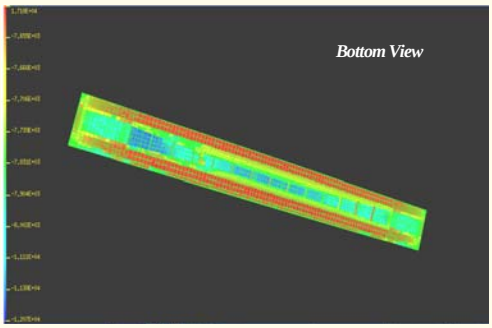

Figure 15. Generalized Normal Stress N_x (lb-in) Distribution after 128,140 Cycles (Fatigue Life) – Bottom View

SUMMARY AND CONCLUSIONS

In this paper, the results of two studies were presented. The first study focused in calibrating the materials constituent properties of the composite army bridge that will be used in demonstrating and virtually verifying the smart repair technology for military bridges. This calibration process is essential in refining both the NASTRAN finite element (FE) and the GENOA Progressive Failure Analytical (PFA) models of the composite army bridge before and after damage as well as after performing the smart repair process. The results of the calibration process identified several variations, especially in the shear moduli, strength and Poisson's ratios. As expected, the original and the calibrated results for unidirectional laminates agreed well.

The second part of the study presented the numerical results that were accomplished using GENOA progressive failure simulation of the composite treadway under three different loading cases. The simulated results matched well the full-scale experimental results reported in Ref. [1]. For the fatigue case, no experimental data were available to compare with the GENOA simulated values.

ACKNOWLEDGEMENTS

This work is a part of an SBIR research project funded by the U.S. Army – TARDEC, Warren, Michigan. The support of Mr. Iyer is highly appreciated. The numerical simulation was conducted jointly by UCI and Alpha Star Corporation under the direction of Dr. Frank Abdi. The information reported in this paper reflects the author' opinions and does not necessary imply endorsement of the sponsored agency.

REFERENCES

1. Advanced Composites for Bridge Infrastructure Renewal-Phase II, DARPA Agreement 0030, Volume II-Task No. MDA972-94-3-14, March 2000, Submitted to DARPA by Advanced Composites Technology Transfer/Bridge Infrastructure Renewal Consortium.
2. Mosallam, A.S. and Haroun, M.A. (2003). "Structural Evaluation, Repair and Construction of a Composite Highway Bridge Deck", *2nd International Workshop on Structural Composites for Infrastructure Applications, NSF/HBRC, Cairo, Egypt, December 17-18, CD ROM*, 2003.
3. Abdi, F., Surdenas, J., Mosallam, A. and Wang, JJ (2003), "Field Repair Technology For Composite Bridges", *Final*

Report, Phase I, Submitted to U.S. Army TACOM, July, 90ps.
4. Murthy, P.L.N. and Chamis, C.C. (1986), "Integrated Composite Analyzer (ICAN): Users and Programmers Manual", *NASA Technical Paper* 2515.
5. Nakazawa, S., Dias, J.B. and Spiegel, M.S. (1987) "MHOST Users' Manual", *Prepared for NASA Lewis Research Center by MARC Analysis Research Corp.*

A New Structural Scheme to Improve the Ductility of FRP Reinforced Concrete Members

by
Y.F. Wu[1] & J.G. Teng[2]

[1]Department of Building and Construction, City University of Hong Kong
yfwu00@cityu.edu.hk
[2]Department of Civil and Structural Engineering, Hong Kong Polytechnic University
cejgteng@polyu.edu.hk

The ductility of FRP reinforced concrete members has been a major concern in the studies of reinforced concrete structures in recent years. Conventional RC members reinforced with ductile bars may also have ductility problems when failure is due to the compressive crushing of concrete without the yielding of the tensile reinforcement; such failure occurs in over-reinforced RC beams and RC columns with a high axial load.

Concrete structures rely largely on the deformation and yielding of the tensile reinforcement to satisfy the ductility demand. In flexural members, when a sufficient rotation of the plastic hinge cannot be achieved through the elongation or the tensile yielding of the reinforcement on the tension side, the other way of achieving it is by shortening or compression yielding (CY) on the opposite compression side. Based on this simple concept, a new method for constructing ductile concrete beams through the use of a CY mechanism has recently been proposed at City University of Hong Kong. The CY scheme involves the application of a ductile compression material or mechanism in the compression zone of the plastic hinge to replace the compressive concrete in a concrete member, as shown in Figure 1.

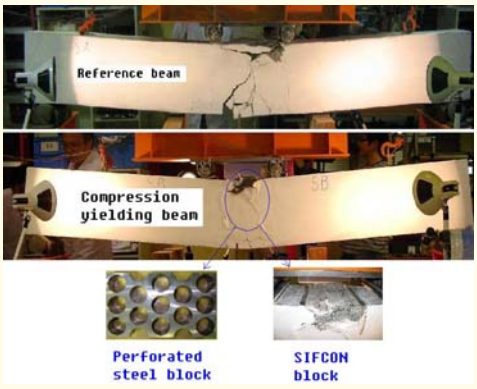

Figure 1. Comparison of Beams

The CY scheme allows the construction of concrete members with great ductility and deformation capacity even when reinforced with brittle tensile bars or subjected to high axial compression.

The only difference between the structural system of a CY beam and that of a conventional RC beam is in the plastic hinge zone where a special ductile compression material or mechanism is used to replace concrete on the compression side. Experimental testing has demonstrated the effectiveness of the new method. In a pilot study, a block constructed from mild steel plates was used to provide the CY mechanism. Test results showed that the CY beam exhibited a much more ductile response; the ductility factor increased from 1.2 of the reference beam that failed by concrete crushing to 2.8 of the CY beam that continued to take significant load at the point where the test had to be stopped due to the travel limit of the test rig.

Further investigations are currently underway, involving collaborations between City University of Hong Kong and The Hong Kong Polytechnic University. The current research focuses on searching for new CY materials and simpler mechanisms. It has recently been found that a perforated steel block (see Figure 1) provides a perfect CY mechanism.

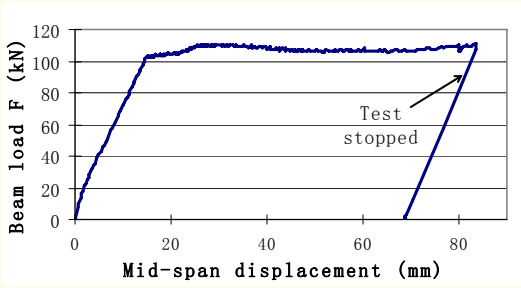

Figure 2. Result of Compression Yielding Beam Test

Figure 2 shows the elastic-perfectly plastic force-displacement response of a simply-supported test beam with a perforated steel block resisting compression at the mid-span. SIFCON (Slurry Infiltrated Fiber Concrete) (Figure 1) has recently been explored as a CY material and the latest results have shown it to be even more promising than the perforated steel block option. SIFCON is not only very strong but also very ductile, and appears to be an ideal material for the CY scheme. SIFCON can be used as normal concrete and a precast SIFCON block can be inserted into the plastic hinge zone of a flexural member to provide sufficient ductility from compression yielding. This new CY technique provides a general solution to the ductility problem of flexural members reinforced with non-ductile bars or subjected to high axial compression.

In this issue we highlight the research facilities at the University of California, Irvine

The Structural Engineering Testing Facilities (SETH) at the University of California, Irvine

by
Ayman Mosallam
University of California at Irvine, Irvine, CA, USA
mosallam@uci.edu

SETH serves as the hub for experimental activities in structural engineering research and is comprised of three major elements: the Structural Engineering Test Hall (SETH), the Shake Table Facility (Bi-Axial Seismic Simulator – BASS) and the Experimental Modal Analysis Laboratory (EMAL). SETH is a 3,500-square feet high bay test hall. Two other labs are being developed; namely; the Advanced Composites and Nano Technology (ACNT) Laboratory directed by Prof. Ayman Mosallam, and the Light Structures Laboratory the will serve the activities and the developments of the ACNT.

The test hall has a strong floor section that is 48 feet wide and 60 feet long. The strong floor is 24 inches thick and has a pass through tie-down holes on a 20-inch grid. A usable basement allows access to the bottom side of the strong floor for attachment of test fixtures and specimens. The basement also provides much needed storage space and the flexibility to mechanize some rather unique test setups. The strong floor is bounded on the east by a strong wall. The strong wall is 22 feet high, 60 feet long and 36 inches thick. The wall is post-tensioned and can safely deliver 150 kip-ft moment per feet of wall length activated. Great care is exercised in the design and execution of experiments to prevent cracking of the strong wall. The interior face of the wall is used for attaching test fixtures and actuators. A useful feature of the strong wall is that it also accessible from the exterior. This feature that has been put to use to quickly and easily mechanize tests in the lab. In addition, this feature allows testing to be conducted outside. This is a major thrust of a planned laboratory capability expansion. The test hall is serviced by a 5-ton crane of 24-feet high lift. The crane can travel outside the laboratory to access a portion of the corporate yard thus improving its utility. The 2,500 square feet corporate yard is used for construction and storage. In addition to the crane, hydraulic jacks and machinery rollers have been used, and therefore, specimens up to 25 tons have been constructed, moved and tested. The hydraulic systems that exist in the lab mainly consist of a complete integrated MTS servo-hydraulic test system. It consists of a 70 gpm pump, hydraulic distribution system and rack mounted control system. There are two 55 kip actuators that have dual valve manifolds with single 15 gpm valves, integral displacement and load transducers. There are also two 220 kip fitted with 90 gpm valves. It is proposed to upgrade these existing 220 kip actuators, taking advantage of their expensive components to achieve greatly improved performance while minimizing cost. In addition to these servo hydraulic actuators there are various other large bore, long stroke actuators in the lab. The capacities range from 100 to 400 kips. In addition to the main laboratory, there are a variety of support elements. A computer room is adjacent to the test floor area. It serves as a project office, a place for data analysis and a procurement reference library. A dual use room adjacent to the test hall houses other test equipment including a Tinius Olsen 200-kip Universal Testing Machine and a concrete cylinder test rig. An electronics shop allows for quick and easy fabrication and maintenance of wide variety of instrumentation. The laboratory has a large stock of displacement and force transducers. The displacement transducers range from 1 inch to 60 inches. A wealth of attachment fixtures for displacement transducers have been developed and maintained over the years. Load cells from 10 kips to 350 kips are available. Complete strain gauging capabilities are available. A 10-feet x 12-feet shake table with uni-axial horizontal and vertical motion became operational in summer 1999. The table has a unique design and, at the time of purchase, unique capacities. The table has a maximum horizontal stroke of ±10 inches provide by a single actuator set. This displacement is large, if not the largest in the country at the time of purchase. A maximum vertical stroke of ±5 inches is provided by 4 actuators sets. Two of these actuator sets are hydraulically slaved to effectively create a single actuator. This achieves the goal of providing "three" vertical actuators thus preventing vertical actuators from warping the tabletop. Each actuator set consists of two single acting actuators and a servovalve. Each actuator can only push but since they are implemented in pairs; one single acting actuator "retracts" the other single acting actuator. Because of the "split actuator" design there are no long actuator bodies, thus eliminating potentially troublesome actuator bending modes. The split actuator design allows for a very compact shake table base, simplifying installation and reducing cost. Additionally there is no kinematics cross coupling between horizontal and vertical motions thus simplifying control issues. The shake table is capable of producing nearly 1.0 g horizontal excitation at 1 Hz for a 20,000 lb. test article. Much heavier specimens (up to 50,000 lb) can be safely tested on the table but at reduced horizontal acceleration due to actuator force limitations. EMAL is used for experimental vibration research and teaching. The lab is equipped with several dual-channel dynamic signal analyzers. It also has several PC and UNIX based multi-channel data acquisition, some specifically designed for rapid FFT calculations. One of the data acquisition systems has 128 channels of input. An extensive array of force and motion sensors is available. They cover a wide frequency range, seismic to acoustic. Dynamic force actuators (10 lb, 30 lb, and 100 lb) and two 5,000-lb eccentric mass shakers can be used to excite structures. Instrumented hammers are available for impact testing. A small horizontal shake table was fabricated in-house for scale model testing and instructional purposes. Workstations have software to perform system identification as well as structural dynamics modification and forced response simulation studies ("what if?" analysis) from the experimentally derived vibration data.

The Structures program at UCI emphasizes the application of analytical and experimental approaches to the investigation of the effects of earthquakes and other extreme hazards on constructed facilities. In graduate programs, students study earthquake magnitude, intensity and frequency; seismic damage to structures; load prediction including response spectra, normal mode and direct integration techniques as well as seismic response for special structures and lifeline engineering. The Structural Engineering Laboratories at UCI serve as the hub for experimental activities in earthquake research and education and are comprised of three major elements; the Structural Engineering Test Hall (SETH), the Shake Table Facility (Bi-Axial Seismic Simulator – BASS) and the Experimental Modal Analysis Laboratory (EMAL). Note

that soft metric conversions have been utilized in the descriptions below.

SETH is a 326 m^2 high bay test hall. The test hall has a strong floor section that is 15 m wide by 18.5 m long. The strong floor is 0.61 m thick and has pass through tie down holes on a 0.5 m grid. A usable basement allows access to the bottom side of the strong floor for attachment of test fixtures and specimens. The basement also provides much needed storage space and the flexibility to mechanize some rather unique test setups. The strong floor is bounded on the east by a strong wall (6.7 m high by 18.3 m long and 0.91 m thick). A useful feature of the strong wall is that it is accessible from the exterior – this will allow us to conduct experiments on both sides of the wall – thereby maximizing its use. The wall is post-tensioned and can safely deliver 670 kN-m moment per meter of wall length activated. SETH is serviced by a 45 kN overhead crane with 7.3 m of lift height. The crane can travel outside the laboratory to access a portion of the corporate yard thus improving its utility. The 232 m^2 corporate yard area is used for construction and storage. The crane capacity is somewhat limited but that limitation has been overcome by the use of hydraulic jacks and machinery rollers. Using this technique, specimens up to 220 kN have been constructed, moved and tested.

The hydraulic systems in SETH primarily consist of a complete integrated MTS servo-hydraulic system, consisting of a 265 LPM pump, a hydraulic distribution system and an integrated rack mounted control system. Currently, available are two 245 kN dynamically rated actuators with dual servovalve manifolds and a single 57 LPM servovalve in-place, integral displacement and load transducers. Also available are two 980 kN dynamically rated actuators fitted with 340 LPM servovalves. In addition to these servo-hydraulic actuators there are various other large bore, long stroke (static) actuators in the laboratory. These capacities range from 445 kN to 1780 kN.

In addition to the main SETH laboratory, there are a variety of support elements. A control room is adjacent to the test floor area. It serves as a project office, a place for data analysis and a procurement reference library. A dual use room adjacent to the test hall houses other test equipment including a Tinius Olsen 890 kN Universal Testing Machine and a concrete cylinder test rig. Undergraduate students within SETH have constructed a complete electronics laboratory. This shop allows for quick and easy fabrication and maintenance of a wide variety of instrumentation. The laboratory has a large stock of displacement and force transducers. Displacement transducers range in stroke from 25 mm to 1500 mm. A wide range of attachment fixtures for displacement transducers have also been developed and maintained over the years. Load cells from 45 kN to 1560 kN are available. The majority of these load cells were purchased as aerospace surplus or fabricated and instrumented in-house. Complete strain gauging capabilities are available.

A 3.1 m by 3.7 m shake table with uni-axial horizontal and vertical motion became operational in Summer 1999. The table has a unique design and, at the time of purchase, unique capacities. The table has a maximum horizontal stroke of ±254 mm provide by a single actuator set. A maximum vertical stroke of ±130 mm is provided by four actuators sets. Two of these actuator sets are hydraulically slaved to effectively create a single actuator. This achieves the goal of providing "three" vertical actuators thus preventing vertical actuators from warping the tabletop. Each actuator set consists of two single acting actuators and a servo-valve. Each actuator can only push but since they are implemented in pairs; one single acting actuator "retracts" the other single acting actuator. Because of the "split actuator" design there are no long actuator bodies, thus eliminating potentially troublesome actuator bending modes. The split actuator design allows for a very compact shake table base, simplifying installation and reducing cost. Additionally there is no kinematic cross coupling between horizontal and vertical motions thus simplifying control issues. The shake table is capable of producing nearly 1.0 g horizontal excitation at 1 Hz for a 90 kN specimen. Much heavier specimens up to 220 kN may be safely tested on the table but at reduced horizontal acceleration due to actuator force limitations.

Experimental Modal Analysis Laboratory (EMAL) is used for experimental vibration research and teaching. This laboratory is equipped with several dual-channel dynamic signal analyzers. It also has several PC and UNIX-based multi-channel data acquisition systems, some specifically designed for rapid FFT calculations. One of the data acquisition systems has 128 channels of input. An extensive array of force and motion sensors is available. They cover a wide frequency range, seismic to acoustic. Dynamic force actuators (45 N, 130 N and 445 N) and two 22kN eccentric mass shakers may be used to excite structures. Instrumented hammers are available for impact testing. A small horizontal shake table was fabricated in-house for scale model testing and instructional purposes. Workstations have software to perform system identification as well as structural dynamics modification and forced response simulation studies from the experimentally derived vibration data. In addition, UCI has a Quasar uni-axial shake table as part of its commitment to the NSF-educational shake table program (UCIST).

CICE Update

The composites community worldwide is looking forward to the upcoming IIFC conference, the 3rd International Conference on FRP Composites in Civil Engineering (CICE 2006) in Miami, FL, December 13-15, 2006. With a total of 165 papers received from over 30 countries, the conference promises to be an excellent forum to exchange ideas and to progress the field of composites in civil engineering.

The three-day conference will include a general session each morning, continued with parallel sessions, coffee breaks in the morning and afternoon and a luncheon with a feature speaker everyday. The conference will also include a reception by the Miami River, a dinner banquet, a pre-conference workshop and a post-conference cruise. Keynote speakers from around the world will discuss prognosis of FRP in construction from the point of view of the research community, funding agency, repair industry, manufacturer, and government users. The conference will tackle issues such as sustainability in construction with FRP and the new frontiers in organic fibers and nano-composites. Miami, often called the "Capital of the Americas" is well known for its hot sunlight, sparkling sand, palm trees, skyscrapers, the beautiful blue ocean, and an internationally diverse culture. The conference will be held at the Hyatt Regency at Miami Convention Center, by the water and a breeze away from the South Beach, at a deeply discounted room rate of only $149 per night.

For additional information, please visit the conference website: http://www.iifc-hq.org/cice2006/

INTERNATIONAL INSTITUTE FOR FRP IN CONSTRUCTION